A high-precision system of fiber Bragg grating temperature sensing demodulation based on light power detection*

HUANG Shuyan[1], HU Xiaohua[1], ZHANG Hao[1,2,3], CHEN Weijuan[1], HUANG Youping[1], and FAN Mengyi[1]**

1. Department of Electronic Information Science, Fujian Jiangxia University, Fuzhou 350108, China

2. University of Chinese Academy of Sciences, Beijing 100059, China

3. Fujian Provincial Key Laboratory for Advanced Micro-nano Photonics Technology and Devices, Quanzhou Normal University, Quanzhou 362000, China

(Received 18 February 2022; Revised 28 April 2022)

A system of fiber Bragg grating (FBG) temperature sensing demodulation based on light power detection is proposed in this paper. Compared with the traditional demodulation method based on wavelength scanning, light power detection is more direct and avoids the use of spectrometer. Moreover, the light power in the system is converted into the electrical signal by the receiver optical subassembly (ROSA) and converted to the digital signal. The micro controller unit (MCU) processes the digital signal to realize the real-time temperature monitoring, which avoids the use of optical power meter (OPM). With the advantages of simple structure and low cost, the system is portable and practical. The experimental results show that the linearity coefficients *R*-square between light power and the sampling voltage are 0.999 08 and 0.998 93 in the temperature range from 10 °C to 85 °C, respectively. According to the results, the proved sensor has a repeatability error of 1%, a linearity error of 1.35%, and a hysteresis error of 0.7%, which indicates that the system is of high stability and high precision. The experimental results are consistent with the theory, which verifies the system's feasibility.

Document code: A **Article ID:** 1673-1905(2022)08-0461-7

DOI https://doi.org/10.1007/s11801-022-2025-6

The fiber Bragg grating (FBG) sensors are actively under investigation for the advantages of strong anti-interference, corrosion resistance, lightweight, and softness[1-4]. Compared with electronic sensors, FBG is passive and more secure without poor battery life or electric spark[5-8]. The parameters of temperature in FBG are converted into the wavelength shift. As a result, wavelength demodulation is the key technology in the FBG sensor. The simplest method is measuring the wavelength shift through an optical spectrum analyzer (OSA), such as the Mach-Zehnder interferometer, and the Fabry-Perot interferometer[9-16]. Although the sensors mentioned above can be used for temperature measurement by using an OSA, there are some shortcomings. For example, the Mach-Zehnder interferometer structure cannot be made into a probe structure[9]. The structure of the Fabry-Perot interferometer is poor in stability[10]. Furthermore, the temperature cannot be displayed in real time, and the use of OSA causes the system to have a complex structure and large volume, which is not ideal for use in portable devices.

Researchers have made various attempts to find a demodulation method for the FBG sensors with low cost, simple structure, and high accuracy[17-20]. Ref.[17] presented a temperature sensor using FBG Fabry-Perot cavity that can be used to discriminate the temperature and strain. However, the demodulation accuracy of the system is reduced by the hysteresis effect of pressurized electric ceramics. Ref.[18] adopted a high-speed fiber grating demodulation technology that benefited from the swept wavelength-tunable laser and single-board computer digital signal processing (DSP) with real-time field programmable gate array (FPGA) processing. However, the demodulation is based on the tunable laser, and the cost is high. Ref.[19] adopted a peak detection algorithm, which should be implemented in distributed FBG and

* This work has been supported by the Natural Science Foundation of Fujian Province of China (Nos.2021J011225, 2021J011224 and 2020J05063), the Key Projects of Industry-University Research Joint Innovation in Colleges and Universities in Fujian Province in 2021 (No.2021H6003), the Fujian Provincial Key Laboratory for Advanced Micro-nano Photonics Technology and Devices, Smart Home Information Collection and Processing on Internet of Things Laboratory of Digital Fujian, and Laboratory for Advanced Sensing Technology of Fujian Jiangxia University.

** E-mail: dream13027@sina.com

Fabry-Perot or Mach-Zehnder interferometer, where the probability of low signal-to-noise ratio (*SNR*) is high. Ref.[20] demonstrated a filterless, temperature-independent FBG dynamical demodulator using pulse width modulation (PWM), which is suitable for a distributed system. However, it is still based on the wavelength shift, which is expensive and difficult to carry.

This paper proposes a system of FBG temperature sensing demodulation based on light power detection to solve the above problems. Theoretical analysis shows that the light power variation of the overlapping spectrum of two FBGs is linear with the temperature. Therefore, compared with the measurement of the wavelength shift, the light power detection is more direct and avoids the use of spectrometer. Meanwhile, the measured temperature is real-time monitored after photoelectric conversion and decoding by the processor, which avoids the use of optical power meter (OPM). The system was established by theoretical analysis and experimented on temperature. The proposed system has the advantages of simple structure, intuition, low cost, portability, and real-time monitoring.

The configuration of the proposed system is shown in Fig.1. The system is composed of an optical signal demodulation path, a photoelectric conversion circuit, and a signal processing circuit. The optical signal demodulation path detects the overlapping spectrum of two chirped FBGs, the FBGA is for the reference, and the FBGB is for sensing. The photoelectric conversion circuit includes a receiver optical subassembly (ROSA) and a sampling resistor to convert the optical signal into a voltage signal. Finally, the signal processing circuit with an analog-to-digital converter (ADC) and micro controller unit (MCU) is to decode and display the measured signal, which avoids the use of OPM.

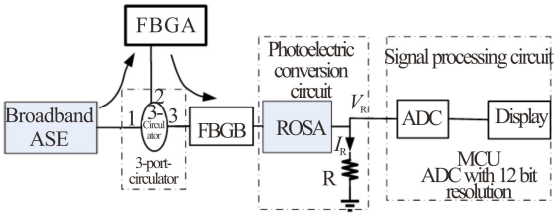

Fig.1 Configuration of the proposed FBG demodulation system

Broadband amplified spontaneous emission (ASE, C-band) light is injected into the FBGA from one port of the 3-port-circulator (port 1), and the reflected signal is injected into the FBGB from port 2 to port 3 of the circulator. FBGB is a temperature-sensitive fiber grating, while FBGA is not sensitive to temperature. Therefore, FBGB is affected by temperature as the sensor, while FBGA is set at room temperature as the reference. On the premise of ignoring the transmission loss, the overlapping spectrum of two FBGs is fixed when FBGA and FBGB are at the same temperature environment, and the transmit light of the FBGB is fixed too. However, when FBGA is at a fixed temperature state, but FBGB is at a various one, the central wavelength of FBGB will shift and result in the overlapping spectrum changing, which is shown in Fig.2.

Moreover, the transmitted light is the wavelength offset of sensing fiber grating caused by temperature change. According to the positive temperature characteristics of FBG, when the central wavelength of FBGB is greater than that of the FBGA (as shown in Fig.2(b)), the transmitted light increases. On the contrary, the transmitted light decreases (as shown in Fig.2(c)). If the relationship between the transmitted light power and temperature is specific, temperature demodulation can be based on light power detection. The theoretical analysis and experiments on temperature will be carried out later to verify this principle. The direct power measurement mainly uses the OPM, which has high power consumption and cannot monitor the temperature in real time. Therefore, after optical path demodulation, the signal should be converted to an electrical signal and decoded.

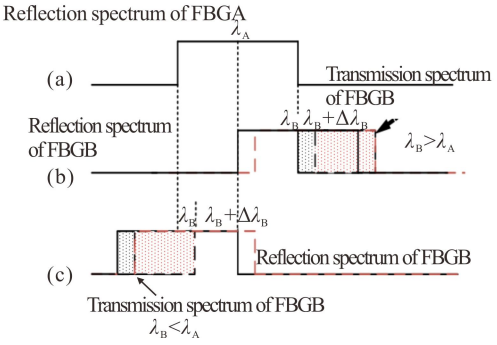

Fig.2 Relationship between reflection spectrum and transmission spectrum of FBGA and FBGB: (a) Reflection spectrum of FBGA; (b) Reflection spectrum and transmission spectrum of FBGB for $\lambda_B>\lambda_A$; (c) Reflection spectrum and transmission spectrum of FBGB for $\lambda_B<\lambda_A$

The photoelectric conversion circuit includes an ROSA and a sampling resistor to convert the optical signal into a voltage signal. The ROSA is a photodiode pin receiver with a super trans-impedance amplifier (TIA). In addition, the module has built-in photodiode pin current monitoring, which can be sampled by a resistor and converted to a voltage. Fig.3 shows the application diagram of the ROSA. The current I_R comes from the 1: 1 mirror image of the pin current. After connecting the sampling resistance R in series, it is converted into voltage V_R for subsequent circuit acquisition.

The signal processing circuit with ADC and MCU is to decode and display the measured signal, which avoids the use of OPM. The ADC with 12 bits is integrated with the MCU, and it has an accuracy of 0.8 mV (ADC power supply voltage is 3.3 V, and its acquisition accuracy is 3.3 V/4 096≈0.8 mV). The ADC collects the voltage V_R

and sends it to MCU, displaying the measured value according to the data fitting characteristics. According to the experiment, when the light source power is 20 mV and the temperature is from 10 °C to 85 °C, the transmitted light power range is from 45.27 μW to 20.53 μW. After the conversion of ROSA, the current value range is from 45.21 μA to 20.19 μA. To meet the accuracy of ADC, we set the sampling resistance R as 48 kΩ, so the voltage range is from 2.17 V to 1.085 V.

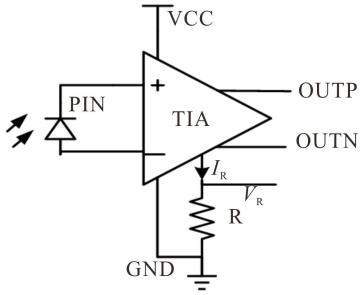

Fig.3 Application diagram of ROSA

According to the characteristics of chirped FBG[21], the reflection wavelength has a positive linear relationship with temperature. Thus, the shift of wavelength affected by temperature can be calculated as follows

$$\Delta\lambda=m\Delta T, \tag{1}$$

where $\Delta\lambda$ and ΔT are the changes of the wavelength and the temperature. m is the temperature coefficient, which is a constant.

According to the principle of power density[22], it can be deduced that the transmission light power of sensing fiber grating (FBGB) in the demodulation system can be calculated as follows

$$P_{\mathrm{T}}=\int_{B_{\mathrm{T}}} P(\lambda)\mathrm{d}\lambda \approx \frac{B_{\mathrm{T}}}{B_{\mathrm{I}}} a_1 P_{\mathrm{I}}, \tag{2}$$

where P_{T} is the transmission light power, P_{I} is the total power of the light source ASE, a_1 is the loss factor of the 3-port-circulator ring port, B_{T} is the half-height width of the FBGB transmission spectrum, and B_{I} is the half-height width of ASE.

When FBGA and FBGB are in the same temperature environment, the overlapping reflection spectrum of the two FBGs should be maintained. However, it is assumed that the central wavelength offset of FBGB is $\Delta\lambda_{\mathrm{B}}$, which is resulting from the change in temperature. Because the transmitted light is caused by the wavelength shift of FBGB as analyzed above, and the wavelength shift is equal to the half-height width of the transmission spectrum, the transmission light power change corresponding to the wavelength offset can be calculated as follows

$$\Delta P_{\mathrm{T}}=\int_{\Delta x} P(\lambda)\mathrm{d}\lambda \approx \frac{\Delta\lambda_{\mathrm{B}}}{B_{\mathrm{I}}} a_1 P_{\mathrm{I}}=\frac{a_1 P_{\mathrm{I}}}{B_{\mathrm{I}}}\Delta\lambda_{\mathrm{B}}=k\Delta\lambda_{\mathrm{B}}, \tag{3}$$

where $k=a_1P_{\mathrm{I}}/B_{\mathrm{I}}$ is a constant. It is deduced that the transmission light power has a linear relationship with the wavelength offset $\Delta\lambda_{\mathrm{B}}$.

Combining Eq.(1) and Eq.(3), we can find out that $\Delta P_{\mathrm{T}}=k\Delta\lambda_{\mathrm{B}}=km\Delta T$. Therefore, the transmission of light power is linear with various temperatures.

A temperature-sensing experiment is conducted based on the setup in Fig.4 to verify the feasibility of the proposed system. The structure comprises an ASE light source, two FBGs, a 3-port-circulator, an ROSA, an MCU embedded ADC, and a heating water tank. The sensing fiber grating FBGB is placed on the heating table, and the reference fiber grating FBGA is placed on the optical platform. The thermometer in the forum monitors the heating water temperature and the room temperature. The FBGA is mainly affected by room temperature, while the FBGB is affected by the heating table. The multimeter displays the sampling voltage compared to the ADC acquisition voltage. When verifying the collected voltage of ADC, it is found that the collected value is 0.03 V less than the actual test value of the multimeter, so a 0.03 adjustment factor is added to the program.

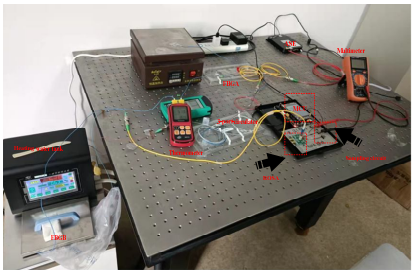

Fig.4 Experimental setup of the proposed system

As described above, FBGB is a temperature-sensitive fiber grating, but FBGA is not sensitive to temperature. Thus, the FBGB (OEFBG, O/E Land Inc., Canada) and the FBGA (OEFBG, O/E Land Inc., Canada) used in the experiment are measured by an OSA (MS9740A, Anritsu, Japan). Fig.5 shows the spectra of the FBGA and the FBGB. As shown in Fig.5(a), the FBGA has a good reflection in the range from 1 550.31 nm to 1 560.05 nm, and the center wavelength is 1 555.08 nm. As shown in Fig.5(b), the FBGB has a good reflection in the range from 1 545.62 nm to 1 555.54 nm, and the center wavelength is 1 550.6 nm. To further analyze the effectiveness and consistency of the system, the temperature coefficient of the FBG should be tested. Fig.6 shows the central wavelength of the FBG with temperature variations. As shown in Fig.6(a), the temperature coefficient of the FBGA is 4.93 pm/°C in the range from 10 °C to 85 °C. As shown in Fig.6(b), the thermal sensitivity of FBGB is a bit low above 85 °C, and the temperature coefficient is 16.4 pm/°C in the temperature range from 10 °C to 85 °C. Fig.6(b) shows that the linearity of the sensitive FBGB is good in the range from 10 °C to 85 °C, so we test the temperature from 10 °C to 85 °C. A sensitized fiber grating with a broader temperature range is needed if you want to increase the test range. The output power of the ASE (ASE-C-20-2-0-1-M, MAX-RRY-PHOTONIC-S, China) is 20 mW. Fig.7 shows the spectrum of the ASE source. It shows that the flatness of the spectrum is less than 3 dB from

1 526.6 nm to 1 565.2 nm, which covers the C-band. To reduce the system's nonlinearity, the wavelength range of the FBGs should be within the wavelength range of the ASE. The ROSA (EOC1089, EOCHIP, China) is with low power consumption and high sensitivity. The wavelength range of receiving light is from 1 490 nm to 1 570 nm, and the sensitivity is −31 dBm.

To verify the relationship between the temperature and the transmitted light power of the FBGB, a calibration experiment should be taken with an OPM (THORLABS, PM320E, USA). In the experiment, adjust the heating water temperature from 10 °C to 85 °C in steps of 1 °C, and record results while the heating temperature and transmitted light power are stable. We record ten data groups at each temperature point and take the average value. The transmitted light power with temperature variation is shown in Fig.8. The *R*-square of linear fitness is 0.999 08, and the proposed sensor's temperature coefficient is 0.321 7 μW/°C.

Then the transmitted light of FBGB is injected into the optical receiving module (ROSA) and converted into current. The current is converted into voltage by the series resistance. The voltage collected by the ADC circuit is sent to the processor for modification and storage. In the experiment, adjust the heating water temperature from 10 °C to 85 °C in steps of 1 °C, and record results while the heating temperature and the voltage are stable. The MCU will average the voltage collected by ADC for ten times at each temperature point and then display the mean voltage. To analyze the stability of the system, we change the temperature of the water box from 10 °C to 85 °C in steps of 1 °C and then change the temperature of the water box from 85 °C to 10 °C in steps of 1 °C. This experiment is repeated five times. We record the results while the temperature and sampling voltage are stable, and process the experiment data by Origin 2018. The five groups of sampling voltages with temperature variations are shown in Fig.9. The temperature variation trend is consistent. The repeatability error of the sensor can be calculated as follows[23]

$$\xi_{\mathrm{R}} = \frac{\Delta S_{\max}}{y_{\mathrm{FS}}} \times 100\%, \tag{4}$$

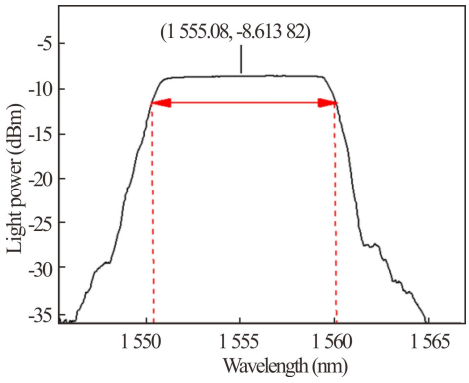

(a) Reflection spectrum of FBGA

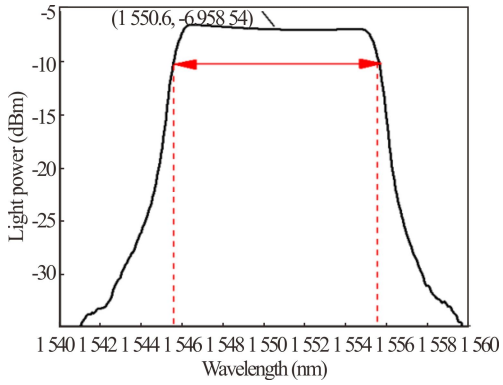

(b) Reflection spectrum of FBGB

Fig.5 Reflection spectra of the FBGA and FBGB

where $\Delta S_{\max}$ is the maximum difference between the results of multiple measurements, and y_{FS} is the system's full-scale output. The maximum standard deviation is about 31.53 mV, and the system's full-scale output is 1.098 1 V. Therefore, the repetitiveness is 2.871%.

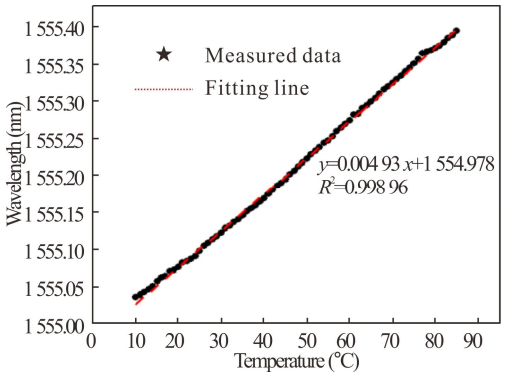

(a) Temperature coefficient of the FBGA

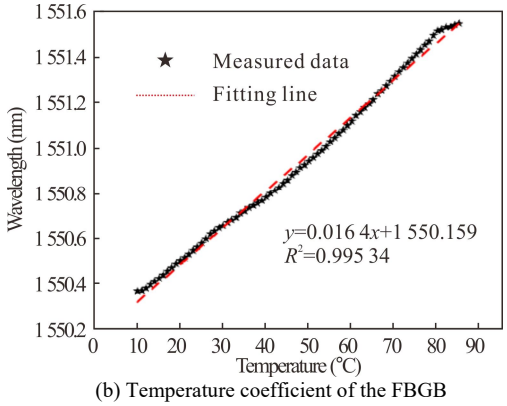

(b) Temperature coefficient of the FBGB

Fig.6 Temperature coefficients of the FBGA and FBGB

Fig.10 shows the average results with the error bar and the linearly fitted relationship curve. As shown in Fig.10, the error trend is consistent with that in Fig.9. The maximum difference between the actual measurement results and the linear curve fitting is about 41.02 mV. The maximum difference between the heating and cooling measurements results is about 60.09 mV. Meanwhile, the system's full-scale output is 1.124 1 V. Therefore, the

linearity error of the sensor can be calculated as follows[24]

$$\delta = \frac{\Delta y_{\max}}{y_{\mathrm{FS}}} \times 100\%, \tag{5}$$

where $\Delta y_{\max}$ is the maximum difference between the actual measurement results and the linear curve fitting. The hysteresis error of the sensor can be calculated as follows[25]

$$\xi_{\mathrm{H}} = \frac{\left| y_{\mathrm{Hi}} - y_{\mathrm{Li}} \right|_{\max}}{y_{\mathrm{FS}}} \times 100\%, \tag{6}$$

where $\left| y_{\mathrm{Hi}} - y_{\mathrm{Li}} \right|_{\max}$ is the maximum difference between the heating measurement results and the cooling measurement results at a certain point. Thus, the measurement results in Fig.10 have a linearity error of 3.65% and a hysteresis error of 5.34%, which indicates that the system is highly stable. As shown in Fig.10, the *R*-square of linear fitness is 0.998 93, suggesting that the measured result has a good consistency and can be repeated. The temperature coefficient of the proposed sensor is 14.9 mV/°C, which can meet the accurate acquisition of the ADC. Through repeated measurement, it is found that the variation trend of voltage with temperature is consistent with the transmitted light power, which shows that the linearity of the photoelectric conditioning circuit is good.

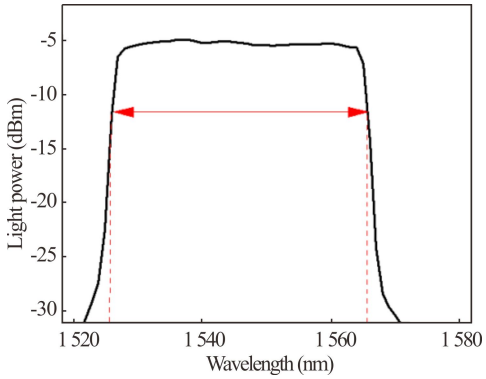

Fig.7 Reflection spectrum of the ASE light source

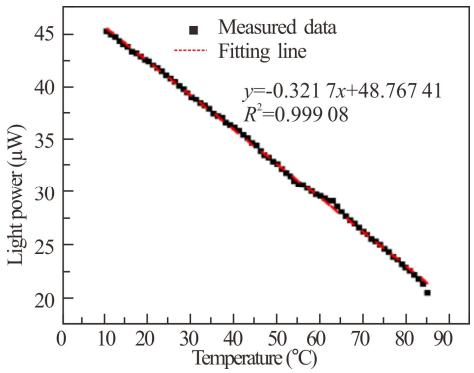

Fig.8 Transmitted light power versus temperature

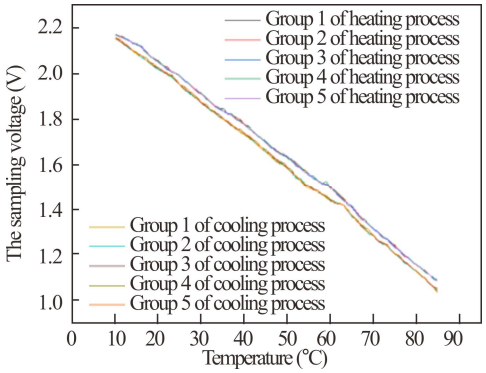

Fig.9 Five groups of sampling voltages versus temperature

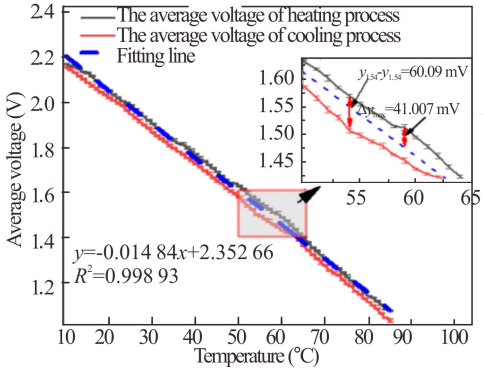

Fig.10 Linear fitting of the temperature sensing results with error bar

A good agreement is observed between theoretical analysis and experimental results. The minor differences between values can be attributed to the limitations of the experimental setup and the relatively low number of measured samples. The relationship between the voltage and the temperature can be calculated as follows

$$y = -0.014\,84x + 2.352\,66, \tag{7}$$

where y is the sampling voltage by the ADC and x is the temperature. Then the MCU transforms the voltage to the temperature and displays the measured value. Fig.11 shows the measured temperature of the system. The temperature is measured in the range from 10 °C to 85 °C in steps of 1 °C, including the heating and the cooling process. The data are average results, and error bars are also shown. It shows that the maximum difference between the actual measurement results and the linear curve fitting is about 1.012 48 °C, the maximum difference between the heating measurement results and the cooling measurement results is about 0.573 97 °C, and the system's full-scale output is 75 °C. Thus, the measurement results in Fig.11 have a linearity error of 1.35% and a hysteresis error of 0.7%. As shown in Fig.11, the *R*-square of linear fitness is 0.999 75, and the slope is 0.984 98. Therefore, the temperature sensitivity of the system is 98.498%, which indicates that the sensor is with high precision. In repeated experiment, we find out the displayed temperature is dynamic, and the maximum standard deviation is about 0.752 31 °C, so the

sensor's repetitiveness is about 1%. The leading cause of temperature error is the acquisition voltage jump caused by the unstable light source and the effect of the vibration of the optical platform. Meanwhile, it is also affected by the roughness caused by measurement in steps of 1 °C. Therefore, the accuracy needs to be further improved. However, the demodulated temperature changes linearly with the set value, which verifies the effectiveness and feasibility of the system.

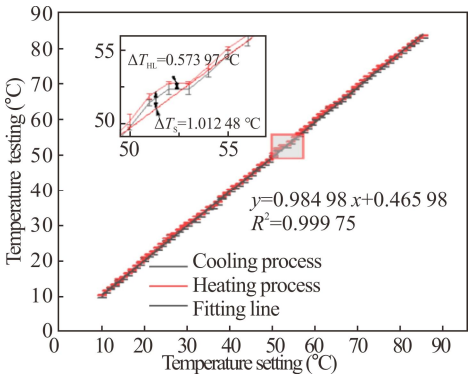

Fig.11 Contrast of the demodulated temperature and the set temperature

An FBG temperature sensing demodulation system is proposed based on light power detection. The temperature demodulation is realized by measuring the light power of the overlapping spectrum of the two FBGs. The system was established by theoretical analysis and experiment on temperature. The experimental results show that the linearity coefficients *R*-square between light power and the sampling voltage are 0.999 08 and 0.998 93 in temperature range from 10 °C to 85 °C, respectively. According to the results, the proved sensor has a repeatability error of 1%, a linearity error of 1.35%, and a hysteresis error of 0.7%, which indicates that the system is of high stability and high precision. However, the temperature error is within 1 °C, which should be improved by selecting a thermostat with uniform heating or an FBG with higher temperature sensitivity. Compared with the wavelength scanning method, the proposed system has the advantages of simple design, low cost, portability, and real-time monitoring without the spectrometer or power meter.

Statements and Declarations

The authors declare that there are no conflicts of interest related to this article.

References

[1] HILL K O, FUJII Y, JOHNSON D C, et al. Photosensitivity in optical fiber waveguides: application to reflection filter fabrication[J]. Applied physics letters, 1978, 32(10): 647-649.

[2] ZHANG F X, JIANG S D, WANG C, et al. Broadband and high sensitivity FBG accelerometer based on double diaphragms and H-shaped hinges[J]. IEEE sensors journal, 2021, 21(1): 353-359.

[3] DAR A B, JHA R K. Chromatic dispersion compensation techniques and characterization of fiber Bragg grating for dispersion compensation[J]. Optical and quantum electronics, 2017, 49(3): 1-4.

[4] PENG C, ZENG C, WANG Y. Phase-based non-contact vibration measurement of high-speed magnetically suspended rotor[J]. IEEE transactions on instrumentation and measurement, 2020, 69(7): 4807-4817.

[5] HONG C Y, ZHANG Y F, ZHANG M X, et al. Application of FBG sensors for geotechnical health monitoring, a review of sensor design, implementation methods and packaging techniques[J]. Sensors and actuators A: physical, 2016, 244: 184-197.

[6] WANG Y L, TU Y, TU S T. Development of highly-sensitive and reliable fiber Bragg grating temperature sensors with gradient metallic coatings for cryogenic temperature applications[J]. IEEE sensors journal, 2021, 21(4): 4652-4663.

[7] YOSHINO T, SANO Y, OHTA D, et al. Fiber-Bragg-grating based single axial mode Fabry-Perot interferometer and its strain and acceleration sensing applications[J]. Journal of lightwave technology, 2016, 34(9): 2241-2250.

[8] MASSIMO L F, MARCO P, ANGELO C, et al. Triaxial fiber optic magnetic field sensor for magnetic resonance imaging[J]. Journal of lightwave technology, 2017, 35(18): 3924-3933.

[9] XIAO S Y, WU B L, WANG Z X, et al. A peanut taper based Mach-Zehnder interferometric sensor for strain and temperature discrimination[J]. Optical fiber technology, 2022, 70: 102871.

[10] ZHANG C, FU S, TANG M, et al. Femtosecond laser fabricated all-multicore-fiber parallel Fabry-Perot interferometers for dual-parameter sensing[C]// Proceedings of the Optical Fiber Communication Conference and Exhibition, March 8-12, 2020, San Diego, CA, USA. New York: IEEE, 2020: 8-12.

[11] OU Y W, ZHOU C M, QIAN L, et al. Large WDM FBG sensor network based on frequency-shifted interferometry[J]. IEEE photonics technology letters, 2017, 29(6): 535-538.

[12] YURIY S, AZAT M. Measurement of spectra of fiber Bragg gratings by tuning the wavelength of a laser diode[J]. Optics & laser technology, 2022, (151): 108048.

[13] YAN M, YAO M Y, ZHANG H M, et al. En/decoder for spectral phase-coded OCDMA system based on amplitude sampled FBG[J]. IEEE photonics technology letters, 2008, 20(9): 788-790.

[14] ZHANG W, ZHUANG W, DONG M, et al. Dual-parameter optical fiber sensor for temperature and pressure discrimination featuring cascaded tapered-FBG and ball-EFPI[J]. IEEE sensors journal, 2019, 19(14): 5645-5652.

[15] HOU Y R. Research and implementation of high-speed fiber Bragg grating demodulation system[D]. Wuhan：Wuhan University of Technology, 2019：23-25. (in Chinese)

[16] LI H Q, LI Y, LI E B, et al. Temperature-insensitive arrayed waveguide grating demodulation technique for fiber Bragg grating sensors[J]. Optics laser technology, 2013, 51：77-81.

[17] LI G, JI L T, LI G Q, et al. High-resolution and large-dynamic-range temperature sensor using fiber Bragg grating Fabry-Pérot cavity[J]. Optics express, 2021, 29(12)：18523-18529.

[18] ZHAN Y G, LIN F, SONG Z K, et al. Applications and research progress of optical fiber grating sensing in thermoplastic composites molding and structure health monitoring (Article)[J]. Optik, 2021, 229：166122.

[19] DHANALAKSHMI S, NANDINI P, RAKSHIT C, et al. Fiber Bragg grating sensor-based temperature monitoring of solar photovoltaic panels using machine learning algorithms[J]. Optical fiber technology, 2022, 69：102831.

[20] ROSOLEM J B, ARGENTO M C, BASSAN F R, et al. Demonstration of a filterless, multi-point, and temperature-independent fiber Bragg grating dynamical demodulator using pulse-width modulation[J]. Sensors, 2020, 20(20)：5825-5833.

[21] KONNOV A K, MIKHNEVA A A, GRIBAEV A I, et al. Inscription and investigation of the spectral characteristics of chirped fiber Bragg gratings[J]. Journal of optical technology, 2018, 85(9)：531-534.

[22] ZHANG H, JIANG J Z, LIU S, et al. Overlap spectrum fiber Bragg grating sensor based on light power demodulation[J]. Sensors, 2018, 18(5)：1597-1608.

[23] LI H L, XU G, GUI X, et al. An FBG displacement sensor in deformation monitoring of subway floating slab[J]. IEEE sensors journal, 2020, 21：2963-2971.

[24] YANG S J, WU D, WANG Z Y, et al. A CMOS stress sensor chip with integrated signal processing circuits[C]//14th IEEE Sensors, November 1-4, 2015, Busan, Korea. New York：IEEE, 2015：1-5.

[25] ZHENG W X, TANG Z F, YANG C Q, et al. A hysteresis compensation method of magnetostrictive displacement sensor based on the Preisach model[J]. Chinese journal of scientific instrument, 2021, 42(5)：79-89. (in Chinese)